

A MATHEMATICAL MODEL OF ACUTE INFLAMMATORY RESPONSE TO ENDOTOXIN CHALLENGE

ANIRBAN ROY

Department of Chemical and Petroleum Engineering; University of Pittsburgh
1249 Benedum Hall; Pittsburgh, PA 15261, USA

SILVIA DAUN

Department of Mathematics; University of Pittsburgh
301 Thackeray Hall; Pittsburgh, PA 15261, USA

GILLES CLERMONT

Department of Critical Care Medicine; University of Pittsburgh Medical Center
3550 Terrace Street; Pittsburgh, PA 15261

JONATHAN RUBIN

Department of Mathematics; University of Pittsburgh
301 Thackeray Hall; Pittsburgh, PA 15261, USA

YORAM VODOVOTZ

Department of Surgery; University of Pittsburgh Medical Center
W944 Biomedical Sciences Tower, Pittsburgh, PA 15213

CLAUDIO LAGO

Nationwide Children's Hospital
700 Children's Dr; Columbus, OH 43205

ROBERT S. PARKER

Department of Chemical and Petroleum Engineering; University of Pittsburgh
1249 Benedum Hall; Pittsburgh, PA 15261, USA

Key words and phrases. Mathematical model, Inflammation, Cytokines, Sepsis.
The first author is currently at Medtronic Diabetes, Northridge, CA.

ABSTRACT. The body responds to endotoxins by triggering the acute inflammatory response system to eliminate the threat posed by gram-negative bacteria (endotoxin) and restore health. However, an uncontrolled inflammatory response can lead to tissue damage, organ failure, and ultimately death; this is clinically known as sepsis. Pro-inflammatory mediators (*e.g.*, interleukin-6 ($IL - 6$) and tumor necrosis factor (TNF)) up-regulate the inflammatory response, and anti-inflammatory mediators (*e.g.*, interleukin-10 ($IL - 10$)) down-regulate the inflammatory signals. In this work, an 8-state (8-D) differential equation model of the acute inflammatory response system to endotoxin challenge was developed. Endotoxin challenges at 3 and 12 mg/kg were administered to rats, and dynamic cytokine data for IL-6, TNF, and IL-10 were obtained and used to calibrate the model. Finally, model validation was performed by comparing the model predictions at an endotoxin challenge level of 6 mg/kg with experimental data from rats at the same level. This 8-D model successfully captured the cytokine dynamics after perturbation with endotoxin at various challenge levels, which indicates that the model may provide insight into the interactions between phagocytic cells and pro/anti-inflammatory mediators.

1. Introduction. The body generates an acute inflammatory response to acute biological stress, such as bacterial infection or tissue trauma. This response consists of a well orchestrated cascade of events mediated by several types of cells and effector molecules; the desired outcome of this response is the containment and elimination of invading pathogens and the repair of damaged tissues [1, 2]. Most of the time, the acute inflammatory response subsides and the body returns to a basal state of health. However, an excessive inflammatory response can lead to tissue damage (rather than repair), organ dysfunction, or possibly death [11].

When initiated by infection, such an excessive response is clinically known as sepsis, which is one of the leading causes of death in modern intensive care units [4, 5]. To control the inflammatory response, organisms have developed regulatory mechanisms such as pro- and anti-inflammatory mediators. In general, the pro-inflammatory effectors (*e.g.*, interleukin-6 ($IL - 6$) and tumor necrosis factor α ($TNF(t)$)) up-regulate inflammation and control infections; the anti-inflammatory elements (*e.g.*, interleukin-10 ($IL - 10$)) down-regulate the inflammatory actions, ideally after infection control has been achieved [1]. Both types of mediators contribute to the initiation of tissue repair.

Our previous work focused on either low-order [6] phenomenological or high-complexity [7, 8, 9] models of the inflammatory response cascade. The latter increase biologic accuracy at the expense of possible parameter identifiability concerns, necessitating either significant data requirements or assumptions for mathematical structure and parameter values. In contrast, low-order models may oversimplify the biology, but formal mathematical analysis is facilitated by such structures. Our previously-developed low-order model [6] consisted of an inflammatory stimulus (pathogen) and early-and-late pro-inflammatory mediators which captured a variety of clinically relevant scenarios, including return to health, sterile death (pathogen free), and septic death (pathogen overload). We later extended the model by incorporating anti-inflammatory mediators, based on their value in restoring health and preventing sterile death [10]. Although these models provided insight into key drivers of inflammatory response outcome, they were not calibrated to experimental data. Hence, the existing low-order models provide little insight into quantitatively precise approaches to altering inflammatory responses.

In this work, we synthesize an intermediate-scale model of acute inflammatory response to endotoxin challenge and calibrate the model parameters to data from rat studies. Major pro-inflammatory cytokines like $IL6(t)$ and $TNF(t)$, as well as anti-inflammatory cytokines, like $IL10(t)$ and $C_A(t)$ (a biologically-motivated lumped surrogate representing slow acting anti-inflammatory mediators, such as the Transforming Growth Factor- β 1 (TGF- β 1) cytokine and cortisol) were incorporated in the model. Similar to [10], a non-measurable tissue damage marker was also included in the model to quantify the tissue damage caused due to the endotoxin challenge and activated phagocytic cells ($N(t)$). The primary objective of this work was to ground the intermediate inflammatory response model in experimental data, thereby providing a model that captures the dynamic blood concentrations of the major pro- and anti-inflammatory cytokines resulting from introduction of an endotoxin challenge ($P(t)$) in rats.

2. Materials and Methods.

2.1. Experimental Data. Experiments on three cohorts of Sprague-Dawley rats were performed according to an IACUC-approved protocol at the University of Pittsburgh, Department of Surgery, to study the acute inflammatory response to endotoxin insults at various dose levels. Rats weighed approximately 200 g, and rats received endotoxin (*Escherichia Coli*) at dose levels of either 3, 6, or 12 mg/kg, intraperitoneally. Blood samples were collected when rats were sacrificed at 0, 1, 2, 4, 8, 12, and 24 hr after endotoxin administration (4 rats sacrificed per time point per endotoxin dose level). Concentrations of $IL6$, $IL10$, and TNF were measured in triplicate using commercially available ELISA kits (R & D Systems, Minneapolis, MN).

2.2. Mathematical Model of Acute Inflammation. The acute inflammation model consists of eight ordinary differential equations (ODEs). The dependent variables used in the model include: endotoxin concentration ($P(t)$); total number of activated phagocytic cells ($N(t)$), which includes all the activated immune response cells (such as neutrophils, monocytes, etc.); a non-accessible tissue damage marker ($D(t)$); concentrations of pro-inflammatory cytokines IL-6 ($IL6(t)$) and tumor necrosis factor ($TNF(t)$); concentration of the anti-inflammatory cytokine IL-10 ($IL10(t)$); a tissue damage driven non-accessible IL-10 promoter ($Y_{IL10}(t)$); and a non-accessible state representing slow acting anti-inflammatory mediators ($C_A(t)$).

A schematic diagram of the model capturing all the major interactions between the eight states is shown in Figure 1. Introduction of $P(t)$ into the system activates $N(t)$. Once activated, $N(t)$ up-regulates production/release of all the inflammatory mediators ($TNF(t)$, $IL6(t)$, $IL10(t)$, and $C_A(t)$) [12]. The pro-inflammatory cytokines have a positive feedback on the system; thereby, they further activate N , and up-regulate other cytokines [12, 14]. On the other hand, the anti-inflammatory cytokine and mediators have a negative feedback on the system. Hence, $IL10(t)$ and $C_A(t)$ inhibit the activation of $N(t)$ and up-regulation of other cytokines [15, 16]. The model also incorporates tissue damage due to activated phagocytic cells, represented by a damage marker, $D(t)$. Tissue damage further up-regulates activation of $N(t)$ [18] and also contributes to up-regulation of $IL10(t)$ [19, 20].

The endotoxin insult injected intraperitoneally in the rats is a bolus administration, which initiates the inflammatory cascade. The ODE describing the dynamics

of $P(t)$ can be written as:

$$\frac{dP(t)}{dt} = -d_P \cdot P(t) \quad (1)$$

$P(t)$ decays exponentially with a rate equal to d_P . The decay rate was fixed at 3 hr^{-1} , which is consistent with the values obtained from published literature [3, 24, 25]. The initial conditions ($t = 0$) for Eq. (1) are either 3, 6, or 12 mg/kg depending on the endotoxin dose level.

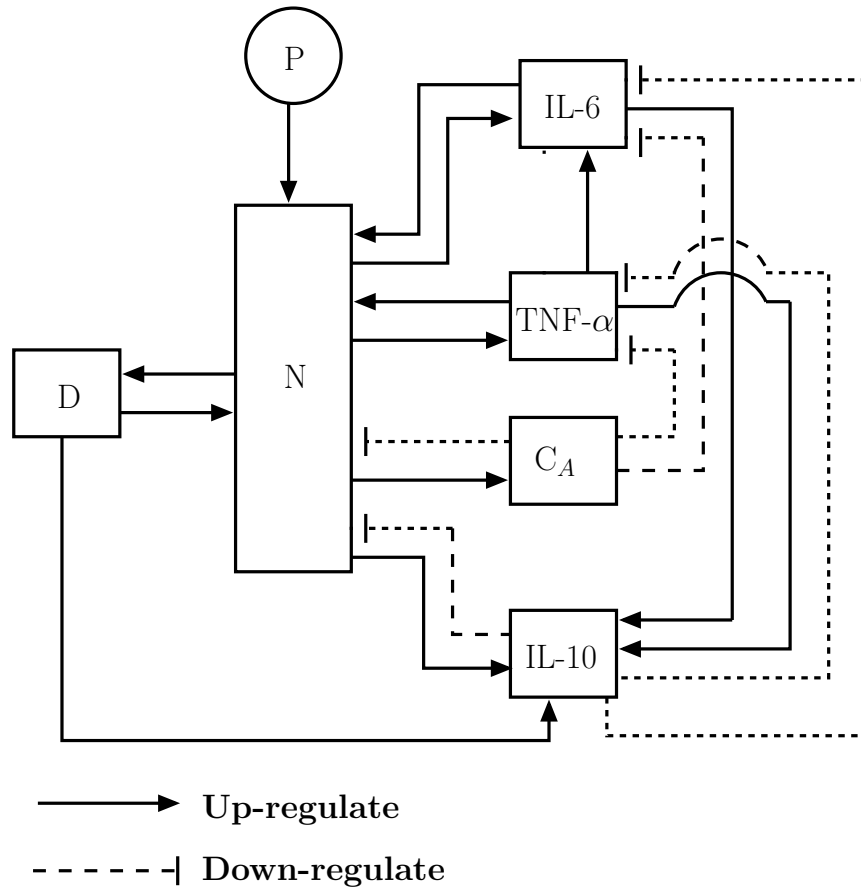


FIGURE 1. Schematic diagram of inflammatory response system challenged by endotoxin

Resting phagocytic cells are activated by the presence of endotoxin in the system. The equations representing activation of $N(t)$ can be mathematically written as:

$$\frac{dN(t)}{dt} = k_N \cdot \frac{R(t)}{x_N + R(t)} - d_N \cdot N(t) \quad (2)$$

$$R(t) = [k_{NP} \cdot P(t) + k_{ND} \cdot D(t)] \cdot [(1 + k_{NTNF} \cdot fUP_{NTNF}(t)) \cdot (1 + k_{NIL6} \cdot fUP_{NIL6}(t))] \cdot fDN_{NCA}(t) \cdot fDN_{NIL10}(t) \quad (3)$$

$$fUP_{NTNF}(t) = \frac{TNF(t)}{x_{NTNF} + TNF(t)} \quad (4)$$

$$fUP_{NIL6}(t) = \frac{IL6(t)}{x_{NIL6} + IL6(t)} \quad (5)$$

$$fDN_{NCA}(t) = \frac{x_{NCA}}{x_{NCA} + C_A(t)} \quad (6)$$

$$fDN_{NIL10}(t) = \frac{x_{NIL10}}{x_{NIL10} + IL10(t)} \quad (7)$$

Here, Eq. (2) represents the total number of activated phagocytic cells ($N(t)$). Parameters k_N and d_N represent the rate of activation and elimination of $N(t)$, respectively. Activation of $N(t)$ is driven by $P(t)$ and $D(t)$, through $R(t)$, as shown in Eq. (3). Throughout this work, functions with nomenclature $fUP_{ij}(t)$ and $fDN_{ij}(t)$ represent up-regulating (UP) and down-regulating (DN) effects of inflammatory mediator j on mediator i . These up- or down-regulating functions are dimensionless and bounded, having values between 0 and 1. Functions, $fUP_{NTNF}(t)$ and $fUP_{NIL6}(t)$ indicate the up-regulating effects of $TNF(t)$ and $IL6(t)$ on $N(t)$, respectively. Both these functions are Michaelis-Menten type equations, as shown in Eq. (4) and (5). As the concentrations increase, the values of the up-regulating functions also increase, approaching 1 asymptotically. Gain parameters k_{NTNF} and k_{NIL6} scale the up-regulating functions $fUP_{NTNF}(t)$ and $fUP_{NIL6}(t)$ to capture the appropriate effects on $N(t)$, respectively. The inhibitory effects of $C_A(t)$ and $IL10(t)$ are captured by the down-regulating functions $fDN_{NCA}(t)$ and $fDN_{NIL10}(t)$, respectively. Here, as the variables increase, the values of the functions decrease, approaching 0 asymptotically (see Eq. (6) and (7)). Parameters x_N , x_{NTNF} , x_{NIL6} , x_{CA} , and x_{NIL10} are the half-saturation constants determining the concentration level of the variables at which the corresponding up-regulating or down-regulating function will reach half of its saturation point. The initial condition ($t = 0$) for Eq. (2) is $N(0) = 0$.

The tissue damage caused by the inflammatory response to endotoxin challenge is modeled as follows:

$$\frac{dD(t)}{dt} = k_D \cdot \frac{N(t)^6}{x_D^6 + N(t)^6} - d_D \cdot D(t) \quad (8)$$

Parameters k_D and d_D represent the rate of generation and the rate of elimination of the non-measurable tissue damage marker, $D(t)$. Elevated $D(t)$ further contributes to the activation of $N(t)$ (3) [18] and production of $IL10(t)$ [19, 20]. Parameter x_D is the half-saturation constant. A 6th-order Hill function was utilized in order to accurately capture the data. Further explanation regarding the choice of the Hill function coefficient is provided in Section 3.3. The initial condition ($t = 0$) for Eq. (8) is $D(0) = 0$.

The anti-inflammatory moderator, $C_A(t)$, represents a combination of various inflammation inhibitory mediators, including the cytokine Transforming Growth

Factor- $\beta 1$ (TGF- $\beta 1$) and cortisol. The $C_A(t)$ equation is written as:

$$\frac{dC_A(t)}{dt} = k_{CA} \cdot N(t) - d_{CA} \cdot C_A(t) + s_{CA} \quad (9)$$

Parameters k_{CA} and d_{CA} represent the rate of $C_A(t)$ production/secretion and clearance, respectively. At basal conditions, the system is assumed to be slightly anti-inflammatory. This was achieved by introducing a constant, s_{CA} , into the ODE. Hence, at $t = 0$ and $N(0) = 0$, $C_A(0) = \frac{s_{CA}}{d_{CA}}$.

The dynamics of IL-6, which is predominantly considered a pro-inflammatory mediator, can be mathematically written as:

$$\begin{aligned} \frac{dIL6(t)}{dt} = & k_{IL6} \cdot \left(\frac{N(t)^4}{x_{IL6}^4 + N(t)^4} \right) \cdot [1 + k_{IL6TNF} \cdot fUP_{IL6TNF}(t) \\ & + k_{IL6IL6} \cdot fUP_{IL6IL6}(t)] \cdot fDN_{IL6IL10}(t) \cdot fDN_{IL6CA} \\ & - d_{IL6} \cdot IL6(t) \end{aligned} \quad (10)$$

$$fUP_{IL6TNF}(t) = \frac{TNF(t)}{x_{IL6TNF} + TNF(t)} \quad (11)$$

$$fUP_{IL6IL6}(t) = \frac{IL6(t)}{x_{IL6IL6} + IL6(t)} \quad (12)$$

$$fDN_{IL6IL10}(t) = \frac{x_{IL6IL10}}{x_{IL6IL10} + IL10(t)} \quad (13)$$

$$fDN_{IL6CA}(t) = \frac{x_{IL6CA}}{x_{IL6CA} + C_A(t)} \quad (14)$$

The up-regulation of $IL6(t)$ production is governed by the activated $N(t)$. Production of $IL6(t)$ is further up-regulated by the presence of elevated $TNF(t)$ and $IL6(t)$ itself, and this is captured by the up-regulating functions fUP_{IL6TNF} and $fUP_{IL6IL6}(t)$, respectively. The inhibitory effects of the anti-inflammatory cytokines were captured by the down-regulating functions $fDN_{IL6IL10}(t)$ and $fDN_{IL6CA}(t)$, respectively. The clearance rate of $IL6(t)$ is represented by the parameter $d_{IL6}(t)$. Once again, Section 3.3 further explains the selection of the Hill function coefficient. Parameters x_{IL6} , x_{IL6TNF} , x_{IL6IL6} , x_{IL6CA} , and $x_{IL6IL10}$ are the half-saturation constants. The initial condition ($t = 0$) for Eq. (10) is $IL6(0) = 0$.

Pro-inflammatory TNF- α concentration can be represented by the following equations:

$$\begin{aligned} \frac{dTNF(t)}{dt} = & k_{TNF} \cdot N(t)^{1.5} \cdot [1 + k_{TNFTNF} \cdot fUP_{TNFTNF}(t)] \\ & \cdot fDN_{TNFCA}(t) \cdot fDN_{TNFIL10} \cdot fDN_{TNFIL6} \\ & - d_{TNF} \cdot TNF(t) \end{aligned} \quad (15)$$

$$fUP_{TNFTNF}(t) = \frac{TNF(t)}{x_{TNFTNF} + TNF(t)} \quad (16)$$

$$fDN_{TNFCA}(t) = \frac{x_{TNFCA}^6}{x_{TNFCA}^6 + C_A(t)^6} \quad (17)$$

$$fDN_{TNFIL10}(t) = \frac{x_{TNFIL10}}{x_{TNFIL10} + IL10(t)} \quad (18)$$

$$fDN_{TNFIL6}(t) = \frac{x_{TNFIL6}}{x_{TNFIL6} + IL6(t)} \quad (19)$$

The rate of production of $TNF(t)$ due to activation of $N(t)$ is governed by the parameter k_{TNF} , and the rate of clearance of $TNF(t)$ is represented by the parameter d_{TNF} . A power of 1.5 was assigned to $N(t)$ instead of a Michaelis-Menten or Hill type expression in order to capture the rapid production and elimination of $TNF(t)$. Further justification for the proposed $TNF(t)$ -state (Eq. (15)) is provided in Section 3.3. The function $fUP_{TNFTNF}(t)$ represents the up-regulating effect of $TNF(t)$ on its own production. The functions $fDN_{TNFCA}(t)$, $fDN_{TNFIL10}(t)$ and $fDN_{TNFIL6}(t)$ represent the inhibitory effect of anti-inflammatory cytokines $C_A(t)$, $IL10(t)$, and pro-inflammatory cytokine $IL6(t)$ (which in some instances, such as this, acts as an anti-inflammatory mediator [21]), respectively. Parameters x_{TNFTNF} , x_{TNFCA} , $x_{TNFIL10}$, and x_{TNFIL6} are the half-saturation constants. A 6th-order Hill function for $fDN_{TNFCA}(t)$ modeled the rapid suppression of C_A on the $TNF(t)$ dynamics. The initial condition ($t = 0$) for Eq. (15) is $TNF(0) = 0$.

The dynamics of $IL10(t)$, which is a strong anti-inflammatory cytokine, can be represented by the following equations:

$$\begin{aligned} \frac{dIL10(t)}{dt} = & k_{IL10} \cdot \left(\frac{N(t)^3}{x_{IL10}^3 + N(t)^3} \right) \cdot [1 + k_{IL10IL6} \cdot fUP_{IL10IL6}(t) \\ & + k_{IL10TNF} \cdot fUP_{IL10TNF}(t)] - d_{IL10} \cdot fDN_{IL10d}(t) \cdot IL10(t) \\ & + Y_{IL10}(t) + s_{IL10} \end{aligned} \quad (20)$$

$$\frac{dY_{IL10}(t)}{dt} = k_{IL102} \cdot \frac{D(t)^4}{x_{IL102}^4 + D(t)^4} - d_{IL102} \cdot Y_{IL10}(t) \quad (21)$$

$$fUP_{IL10IL6}(t) = \frac{IL6(t)^4}{x_{IL10IL6}^4 + IL6(t)^4} \quad (22)$$

$$fUP_{IL10TNF}(t) = \frac{TNF(t)}{x_{IL10TNF} + TNF(t)} \quad (23)$$

$$fDN_{IL10d}(t) = \frac{x_{IL10d}}{x_{IL10d} + IL10(t)} \quad (24)$$

Here, Eq. (20) captures the circulating $IL10(t)$ levels. Unlike the other measured cytokines, the $IL10(t)$ dynamics demonstrate two distinct peaks separated by approximately 4 to 6 *hr* when perturbed by endotoxin challenge. The first surge of $IL10(t)$ production is predominantly attributed to $N(t)$, which is captured by a 3rd-order Hill equation multiplied by the parameter k_{IL10} (first RHS term of Eq. (20)). Production of $IL10(t)$ is further up-regulated by the presence of elevated pro-inflammatory cytokines like $IL6(t)$ and $TNF(t)$, which are represented by the up-regulation functions $fUP_{IL10IL6}(t)$ and $fUP_{IL10TNF}(t)$, respectively. The production of $IL10(t)$ in the basal state is represented by the constant s_{IL10} (as observed in experimental data). Hence, at $t = 0$ and $N(0) = 0$, $IL10(0) = \frac{s_{IL10} \cdot x_{IL10d}}{(d_{IL10} \cdot x_{IL10d} - s_{IL10})}$. It has been shown in a previous study that the rate of elimination of $IL10(t)$ is inversely proportional to the circulating concentration of $IL10(t)$ [22]. This phenomenon is captured by a down-regulating function, $fDN_{IL10d}(t)$, coupled with the parameter d_{IL10} , as shown in Eq. (20). Further discussion of the Eq. (20) structure is presented in Section 3.3.

The second surge in $IL10(t)$ production is attributed to tissue damage $D(t)$ [19, 20], and the dynamics of this D -induced effect are captured by the variable $Y_{IL10}(t)$ in Eq. (20). The dynamics of $Y_{IL10}(t)$ are represented by the ODE (21); here the rate of production of $Y_{IL10}(t)$ is represented by the parameter k_{IL102} coupled with a 4th-order Hill equation (first term in RHS of Eq. (21)), which is driven by $D(t)$.

Once again, this is data-motivated (see the further discussion in Section 3.3). The rate of elimination of $Y_{IL10}(t)$ is given by parameter d_{IL102} . Parameters x_{IL10} , x_{IL102} , $x_{IL6IL10}$, $x_{IL10TNF}$, and x_{IL10d} are the half-saturation constants.

2.3. Parameter Estimation Technique. Some parameters in the model were specified. The clearance rate of endotoxin ($P(t)$) captured by the parameter d_P in Eq. (1) was obtained from the literature [24, 25]. Parameters (s_{CA}) and (s_{IL10}) from Eqs. (9) and (20) were extracted directly from the experimental data, respectively. The rest of the model parameters were estimated by fitting the rat data of the cytokines $IL6$, TNF , and $IL10$ at endotoxin dose challenge levels of 3 and 12 mg/kg , simultaneously.

Inflammation model parameters were estimated using the nonlinear least-squares technique as described in [26]. The normalized residual is obtained as:

$$\chi^2 \equiv \sum_{i=1}^{Q_P} \left[\frac{y_i - y(t_i, \theta_1 \dots \theta_M)}{\sigma_i} \right]^2 \quad (25)$$

Here, y_i is the measured data at time t_i , which has a standard deviation of σ_i . The model prediction is given by $y(t_i, \theta_1 \dots \theta_M)$, where θ_j represent model parameters. Eq. (25) is the objective of a weighted minimization having $(\frac{1}{\sigma_i})^2$ as the weights and θ_j as the degrees of freedom. Q_P is the total number of data points and M is the total number of model parameters. Parameter optimization was performed by using the *fminsearch.m* function from the MATLAB Optimization Toolbox (©2008 The Mathworks Inc., Natick, MA).

Model validation was accomplished by fixing the estimated parameters and simulating the model at an intermediate dose level of 6 mg/kg . Values of inflammation model parameters are provided in Table 1.

2.4. Akaike's Information Criterion (AIC). AIC [27] was employed to establish a quantitative comparison between the proposed inflammation model structure and candidate simplifications. When comparing two models containing different values of M , the model with the lower AIC value is preferred. The value of AIC can be calculated from the following equation [27]:

$$AIC = Q_P \ln \left(\frac{\chi^2}{Q_P} \right) + 2M \quad (26)$$

The criterion may be minimized over choices of M (the number of model parameters) to yield a trade-off between the quality of fit of the model, which lowers the sum squared error (χ^2 from Eq. (25)), and the model's complexity, which is measured by M .

2.5. Parametric Sensitivity by Finite Difference Method. The model parameters in equations (1)-(24), will vary in their effect on state and output dynamics as a function of operating state and time. Sensitivity analysis, as calculated by finite difference [28, 29], is employed to identify the model parameters that have significant impact on model predictions. Though local, this knowledge can be used to inform the design of future experiments for elucidating model dynamics and parameter values. A drawback of finite difference-based sensitivity analysis is that the information is not global, but the constrained nature of the parameter region (parameter estimates will not change sign) makes global analysis highly conservative and beyond the scope of the present study.

TABLE 1. Parameters of the inflammation model.

No.	Parameter	Value	Unit	No.	Parameter	Value	Unit
1	d_p	3	hr^{-1}	24	$x_{IL6IL10}$	1.1818	$\frac{pg}{mL}$
2	k_N	5.5786e7	hr^{-1}	25	k_{IL6IL6}	122.92	-
3	x_N	14.177	$N - unit$	26	x_{IL6IL6}	1.987e5	$\frac{pg}{mL}$
4	d_N	0.1599	hr^{-1}	27	x_{IL6CA}	4.2352	$\frac{pg}{mL}$
5	k_{NP}	41.267	$\frac{N-unit \cdot kg}{mg}$	28	k_{TNF}	3.9e-8	$\frac{pg}{mL}$
6	k_{ND}	0.013259	$\frac{N-unit}{D-unit}$	29	d_{TNF}	2.035	$\frac{pg}{mL \cdot N-unit^{1.5}}$
7	x_{NTNF}	1693.9509	$\frac{pg}{mL}$	30	$x_{TNFIL10}$	2.2198e7	$\frac{pg}{mL}$
8	x_{NIL6}	58080.742	$\frac{pg}{mL}$	31	x_{TNFCA}	0.19342	$\frac{pg}{mL}$
9	x_{NCA}	0.07212	$\frac{pg}{mL}$	32	k_{TNFTNF}	1.0e-10	-
10	x_{NIL10}	147.68	$\frac{pg}{mL}$	33	x_{TNFTNF}	9.2969e6	$\frac{pg}{mL}$
11	k_{NTNF}	12.94907	-	34	x_{TNFIL6}	55610	$\frac{pg}{mL}$
12	k_{NIL6}	2.71246	-	35	$k_{IL10TNF}$	2.9951e-5	-
13	k_D	2.5247	$\frac{D-unit}{hr}$	36	$x_{IL10TNF}$	1.1964e6	$\frac{pg}{mL}$
14	d_D	0.37871	hr^{-1}	37	$k_{IL10IL6}$	4.1829	-
15	x_D	1.8996e7	$N - unit$	38	$x_{IL10IL6}$	26851	$\frac{pg}{mL}$
16	k_{CA}	.154625e-8	$\frac{pg}{mL \cdot hr \cdot N-unit}$	39	k_{IL10}	1.3374e5	$\frac{pg}{mL \cdot hr}$
17	d_{CA}	.31777e-1	hr^{-1}	40	d_{IL10}	98.932	hr^{-1}
18	s_{CA}	0.004	$\frac{pg}{mL \cdot hr}$	41	x_{IL10}	8.0506e7	$N - unit$
19	k_{IL6TNF}	4.4651	-	42	s_{IL10}	1187.2	$\frac{pg}{mL \cdot hr}$
20	x_{IL6TNF}	1211.3	$\frac{pg}{mL}$	43	x_{IL10d}	791.27	$\frac{pg}{mL}$
21	k_{IL6}	9.0425e7	$\frac{pg}{mL \cdot hr}$	44	k_{IL102}	1.3964e7	$\frac{Y_{IL10} - Unit}{hr}$
22	d_{IL6}	0.43605	hr^{-1}	45	d_{IL102}	0.0224	hr^{-1}
23	x_{IL6}	1.7856e8	$N - unit$	46	x_{IL102}	37.454	$D - unit$

The inflammation model can be expressed as a set of Q_x differential equations with Q_x states (x) and M parameters (θ). The Q_x by M parameter sensitivity matrix can be calculated by using the finite difference approximation method, in which the sensitivity coefficients ($s_{i,j}$) are calculated from the difference of nominal and perturbed solutions [28, 29], as follows:

$$s_{i,j}(t) = \frac{\partial x_i(t)}{\partial \theta_j} = \frac{x_i(\theta_j + \Delta\theta_j, t) - x_i(\theta_j, t)}{\Delta\theta_j} \quad (27)$$

where, $i \in [1, Q_x]$, $j \in [1, M]$.

To facilitate direct comparison of responses across different parameters, normalized sensitivity coefficients ($\bar{s}_{i,j}(t)$) are calculated [28]:

$$\bar{s}_{i,j}(t) = \frac{\partial x_i(t)}{\partial \theta_j} \cdot \frac{\theta_j}{x_i} \quad (28)$$

For the evaluation of dynamic sensitivity, an L^2 -norm operation is performed to calculate the relative sensitivity (RS) aggregated over time. RS can be mathematically expressed as:

$$RS_{i,j} = \frac{1}{Q_T} \sqrt{\sum_{k=1}^{Q_T} |\bar{s}_{i,j}(t_k)|^2} \quad (29)$$

Here, t_k ($k \in [1, Q_T]$) are the times when a sample was collected, and Q_T is the number of sample points observed for a given entity (e.g., $IL6(t)$, $TNF(t)$, etc.).

3. Results.

3.1. Parameter Estimation. Simulation studies of the inflammatory response were performed at endotoxin challenge levels of 3 and 12 mg/kg . The diffusion rate of $P(t)$ (endotoxin) into the blood stream was very rapid from the intraperitoneal administration site [23]. Hence, the endotoxin challenge was modeled as an impulse, and $P(t)$ was modeled as a first-order ordinary differential equation with an impulse input as shown in Figure 2 (a). A fast clearance rate of $P(t)$ ($d_P = 3 \text{ hr}^{-1}$ [24, 25]) caused circulating endotoxin levels to approach zero at approximately 2 hr .

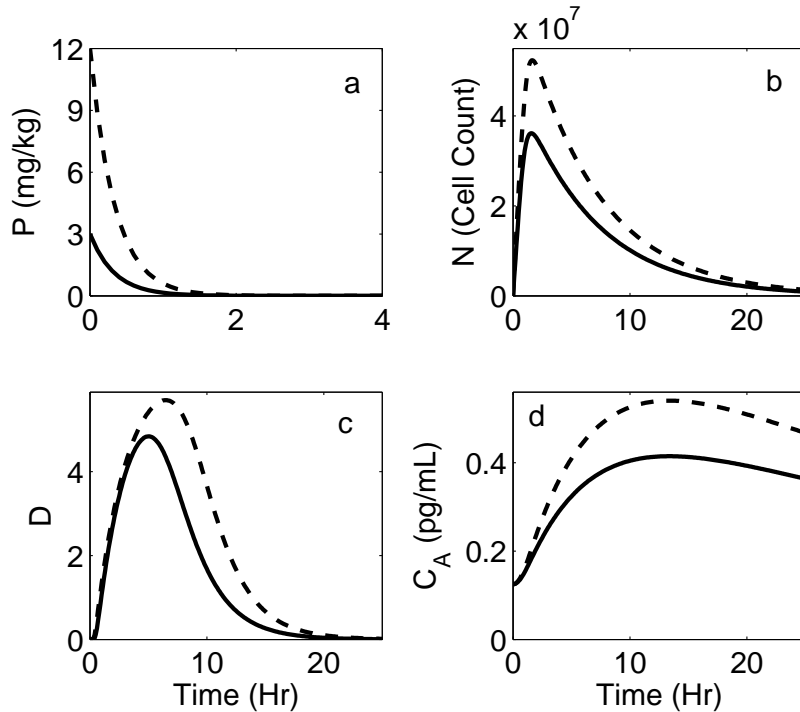


FIGURE 2. Simulation results of inflammation model response to endotoxin challenge level of 3 (solid line) and 12 (dashed line) mg/kg . The abscissa of the top left plot (a) is set at a different time range (0 to 4 hr) than the other plots (0 to 25 hr).

The endotoxin bolus rapidly activates phagocytic cells, as shown in Figure 2 (b). The total cell count, $N(t)$, peaked at $t=1.6 \text{ hr}$ for both endotoxin dose levels. Activation of $N(t)$ caused tissue damage, which is quantified by a unitless tissue damage marker, as shown in Figure 2 (c). Up-regulation of anti-inflammatory moderators, $CA(t)$, as shown in Figure 2 (d), was also a result of $N(t)$.

As an important part of the inflammatory cascade initiated by the endotoxin challenge, the production of $IL6(t)$ was up-regulated by $N(t)$, as shown by the solid lines in Figure 3. The $IL6(t)$ concentration was at its basal level until the first hour post endotoxin challenge. After the initial delay, $IL6(t)$ concentration increased rapidly and peaked at approximately 4 hr for both challenge levels. The model prediction of $IL6(t)$ at both challenge levels fit the data well.

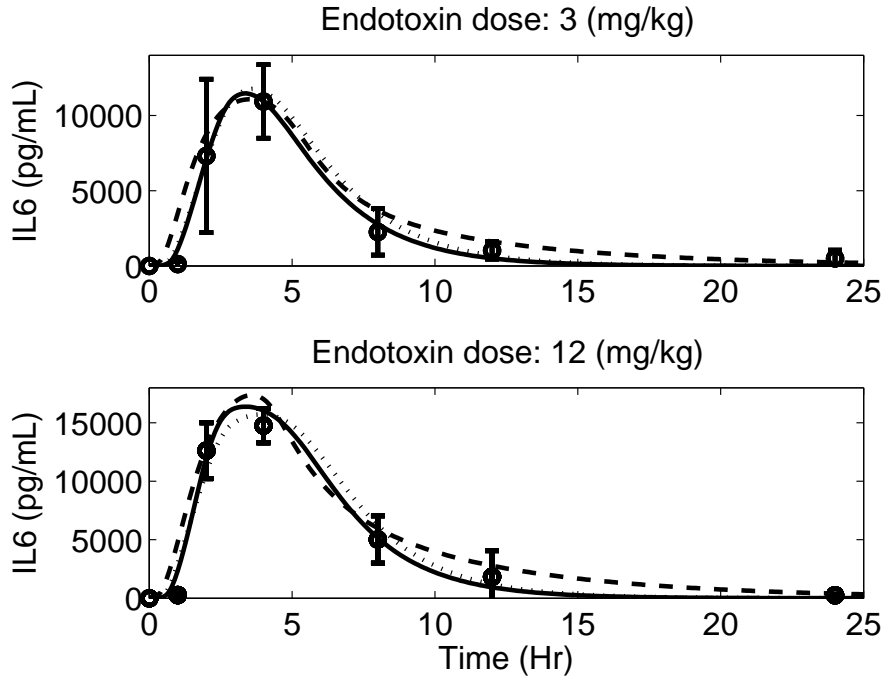


FIGURE 3. Model simulation comparison of IL-6 between the proposed model Eq. (10) (solid line) and its alternate versions, AV-1, Eq. (30) (dashed line) and, AV-2, Eq. (31) (dotted line) against experimental data (circle) (mean \pm SD) in response to endotoxin challenge of 3 mg/kg (top) and 12 mg/kg (bottom).

Production of $TNF(t)$ was up-regulated due to the endotoxin insult. Blood concentration of $TNF(t)$ increased steeply almost immediately after the introduction of the endotoxin challenge, as shown by the solid lines in Figure 4. After peaking at approximately 2 hr for both the challenge levels, $TNF(t)$ concentration decreased rapidly to its basal level, unlike the other measured cytokines. The model predictions of $TNF(t)$ concentration are consistent with the experimental data and are within one standard deviation (SD) of the mean measurement at all time points.

Production of the anti-inflammatory cytokine $IL10(t)$ was also up-regulated by the endotoxin challenge. The dynamics of $IL10(t)$ involved more dynamic features than the other measured cytokines. The solid lines in Figure 5 show that the $IL10(t)$ concentration at both challenge levels had two distinct peaks. The initial production of $IL10(t)$ was mostly up-regulated by $N(t)$, which peaked at approximately 2 hr for both the challenge levels. The latter peak was driven by $D(t)$ and was captured by introducing Eq. (21) in the model. The model predictions of $IL10(t)$ are consistently within one SD of the data, as shown by the solid lines in Figure 5.

3.2. Model Validation. Once all the parameters of the inflammation model were estimated from the 3 and 12 mg/kg endotoxin challenge data (nominal values are shown in Table 1), the model predictions were validated by comparing model simulations with available data at a 6 mg/kg endotoxin challenge level. Parameter

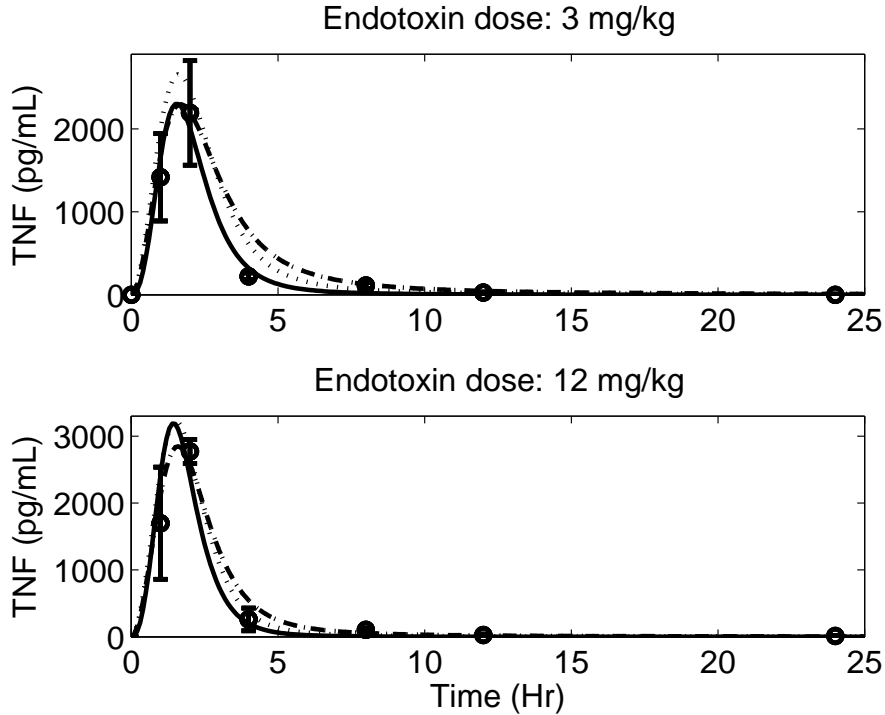


FIGURE 4. Model simulation comparison of $TNF-\alpha$ between the proposed model Eq. (15) (solid line), AV-3 Eq. (32) (dashed line), and AV-4 Eq. (33) (dotted line) against experimental data (circle) (mean \pm SD) in response to endotoxin challenge of 3 mg/kg (top) and 12 mg/kg (bottom).

values were not changed in the validation simulations. Comparison between model predictions and experimental data of $IL6(t)$, $TNF(t)$, and $IL10(t)$ at an endotoxin level of 6 mg/kg are shown in Figure 7.

In general, the model predictions of the measured cytokines were consistent with the experimental data. It can be observed that, in the case of $TNF(t)$ concentration (Figure 7: middle), the data collected at 1 hr is inconsistent with samples collected at the same time point for endotoxin dose levels of 3 and 12 mg/kg . Hence, the model over-predicts $TNF(t)$ at the 1 hr time point. For further evaluation, the 6 mg/kg endotoxin experiment should be repeated to (in)validate the first hour measurement. The model also over-predicts $IL10(t)$ concentration at the last sampling point ($t = 24$ hr) as shown in Figure 7 (bottom); further refinement of the model if the 6 mg/kg data set were employed would focus on reducing the peak shift in $IL10(t)$ at lower challenge doses.

3.3. Model Structure Justification. AIC, as described in Section 3.1, is a widely used statistical method for quantifying the trade-off between model fit and model complexity, as measured by the total number of parameters. While modeling biological systems where a limited number of measured data points are available,

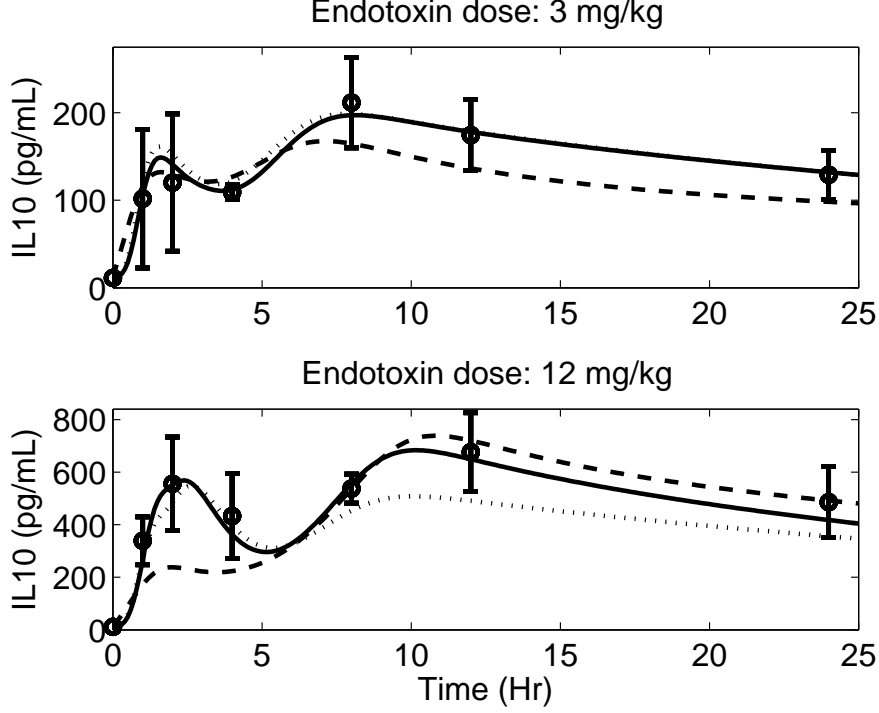


FIGURE 5. Model simulation comparison of IL-10 between the proposed model, Eq. (20), (solid line), AV-5 Eq. (34) (dashed line), and AV-6 Eq. (35) (dotted line) against experimental data (circle) (mean \pm SD) in response to endotoxin challenge of 3 mg/kg (top) and 12 mg/kg (bottom).

over-fitting, over-parameterization, and the introduction of under-justified nonlinearities are significant concerns. Parameter identifiability (*a priori*), estimation quality, and model uniqueness must be addressed when complex models are developed from small data sets. In contrast, compact low parameter count models may be structurally identifiable *a priori*, but they may also yield poor predictive accuracy as measured by model fit (*e.g.*, (weighted) least-squares error). Hence, a balance should be reached in terms of model complexity and accuracy, and AIC provides such a balancing metric.

In modeling $IL6(t)$ with Eq. (10), a 4th-order Hill function ($N(t)^4/(x_{IL6}^4 + N(t)^4)$) was introduced to capture the one hour delay in $IL6(t)$ response to endotoxin challenge. The inclusion of this function was necessary to capture the data accurately (where accuracy is quantitated using Eq. (25)). Addition of this nonlinearity increased the model complexity by one parameter (x_{IL6}) versus a linear-in- $N(t)$ version of Eq. (10) without a Hill function, which can be written as:

$$\frac{dIL6(t)}{dt} = k_{IL6} \cdot N(t) \cdot [1 + k_{IL6TNF} \cdot fUP_{IL6TNF}(t) + k_{IL6IL6} \cdot fUP_{IL6IL6}(t)] - fDN_{IL6IL10}(t) \cdot fDN_{IL6CA} - d_{IL6} \cdot IL6(t) \quad (30)$$

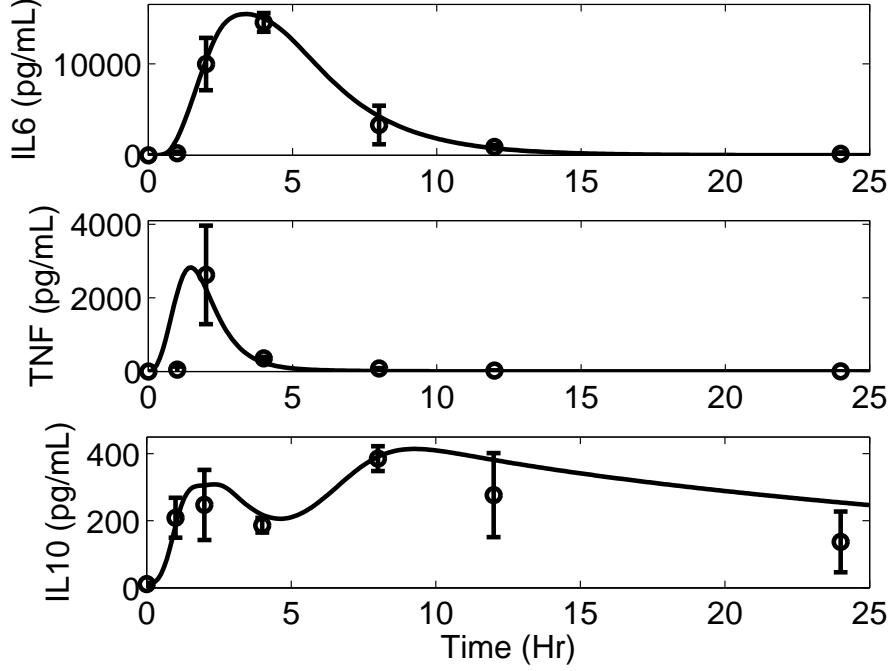


FIGURE 6. Model validation simulation (solid line) of IL-6 (top), TNF- α (middle), and IL-10 (bottom) versus experimental data (circle) (mean \pm SD) in response to endotoxin challenge of 6 mg/kg.

A comparison of $IL6(t)$ predictions from the proposed model (solid line) and an alternate version of the model, AV-1, is provided as the dashed line in Figure 3. Calculated AIC values of both models are given in Table 2. It is clear from the AIC values and the Figure that the nonlinear model is superior to the linear-in- $N(t)$ version.

Furthermore, any Hill function with order < 4 in the $IL6(t)$ state compromised the model accuracy. The $IL6(t)$ state with a 3rd-order Hill function can be written as:

$$\begin{aligned} \frac{dIL6(t)}{dt} = & k_{IL6} \cdot \left(\frac{N(t)^3}{x_{IL6}^3 + N(t)^3} \right) \cdot [1 + k_{IL6TNF} \cdot fUP_{IL6TNF}(t) \\ & + k_{IL6IL6} \cdot fUP_{IL6IL6}(t)] \cdot fDN_{IL6IL10}(t) \cdot fDN_{IL6CA} \\ & - d_{IL6} \cdot IL6(t) \end{aligned} \quad (31)$$

The prediction for model AV-2, in Eq. (31), is provided as the dotted line in Figure 3. Once again, from Table 2 it is evident that the AIC value indicates the superiority of the proposed model over AV-2.

The rapid rise and fall of $TNF(t)$ necessitated the use of two nonlinear terms to capture the dynamic profile. This was primarily captured by assigning the $N(t)$ forcing term a power of 1.5. A second effect included was a 6th-order Hill function for $fDN_{TNFCA}(t)$ in Eq. (17) to rapidly suppress the $TNF(t)$ levels after a challenge. Any order lower than 6 compromised the model accuracy for $TNF(t)$

production, particularly after the 2 *hr* time point. For comparison, a simplified version (eliminating the $N(t)$ nonlinearity) of Eq. (15) can be written as (AV-3):

$$\begin{aligned} \frac{dT_{NF}(t)}{dt} = & k_{TNF} \cdot N(t) \cdot [1 + k_{TNFTNF} \cdot fUP_{TNFTNF}(t)] \\ & fDN_{TNFCA}(t) \cdot fDN_{TNFIL10} \cdot fDN_{TNFIL6} \\ & -d_{TNF} \cdot TNF(t) \end{aligned} \quad (32)$$

The $TNF(t)$ predictions from the proposed model (solid line) and AV-3 (dashed line) are provided in Figure 4. It is evident that the $TNF(t)$ dynamics predicted by AV-3 are not as rapid as that observed in the experimental data. For structural consistency, another version of the $TNF(t)$ -state with a Michaelis-Menten expression was formulated as follows (AV-4):

$$\begin{aligned} \frac{dT_{NF}(t)}{dt} = & k_{TNF} \cdot \left(\frac{N(t)}{x_{TNF} + N(t)} \right) \cdot [1 + k_{TNFTNF} \cdot fUP_{TNFTNF}(t)] \\ & fDN_{TNFCA}(t) \cdot fDN_{TNFIL10} \cdot fDN_{TNFIL6} \\ & -d_{TNF} \cdot TNF(t) \end{aligned} \quad (33)$$

The model prediction from AV-4 (dotted line) is also presented in Figure 4. Once again, it is clear that a Michaelis-Menten formulation, which added an extra parameter (x_{TNF}), is inadequate to capture the fast dynamics of $TNF(t)$ accurately. The calculated AIC values from Table 2 reveal that the proposed model is superior to the two alternate model structures.

The dynamic profile of IL-10 response to the endotoxin challenge justifies further nonlinear terms in the model. The 2-hour data point mean value for the 12 *mg/kg* challenge is 3.6 times higher than that for the 3 *mg/kg* challenge. To capture this nonlinear scaling, a 3rd-order Hill function ($N(t)^3/(x_{IL10}^3 + N(t)^3)$) was used, as shown in Eq. (20). While the inclusion of this nonlinearity added an extra parameter (x_{IL10}), comparison with simpler models demonstrates its need. An alternate linear (in terms of $N(t)$) version of the $IL10$ -state can be written as follows (AV-5):

$$\begin{aligned} \frac{dIL10(t)}{dt} = & k_{IL10} \cdot N(t) \cdot [1 + k_{IL10IL6} \cdot fUP_{IL10IL6}(t) \\ & + k_{IL10TNF} \cdot fUP_{IL10TNF}(t)] - d_{IL10} \cdot fDN_{IL10d}(t) \cdot IL10(t) \\ & + Y_{IL10}(t) + s_{IL10} \end{aligned} \quad (34)$$

This reduced the model complexity by one parameter (x_{IL10}). A comparison of the model predictions from the proposed model (solid lines) and the alternate version (dashed lines) is provided in Figure 5. It is clear that AV-5 is unable to capture the nonlinearities that exist in the $IL10(t)$ dynamics between endotoxin dose levels of 3 and 12 *mg/kg*, especially during the first peak.

IL-10 dynamics after the initial peak, are affected by $IL6(t)$. A 4th-order Hill function for the $fUP_{IL10IL6}(t)$ dynamics (Eq. (22)) was necessary to delay the effects of $IL6(t)$ on $IL10(t)$, as any lower-order Hill expression resulted in a faster elimination of $IL10(t)$ after reaching the first peak thus causing the model to underpredict the $IL10(t)$ dynamics at the 4 *hr* time point.

The tissue damage-mediated second surge of IL-10 concentration required the use of a 6th-order Hill function ($N(t)^n/(x_D^n + N(t)^n)$, where $n = 6$) in Eq. (8). The higher-order Hill function was necessary to accurately capture the second peak in the $IL10(t)$ concentration, which occurred after an initial decrease as observed at

the 4 hr time point in the experimental data. A comparison of model predictions between the proposed model and alternate versions of Eq. (8) represented by 4th-order ($n = 4$), AV-7, and 2nd-order ($n = 2$), AV-8, Hill functions are presented in Figure 6. It is evident that lower-order ($n < 6$) Hill expressions in Eq. (8) result in slower $IL10(t)$ dynamics, especially after the 4 hr time point. The calculated AIC values presented in Table 2 clearly indicate that the proposed model is again superior to these alternate versions, particularly for fitting the 3 mg/kg dose results.

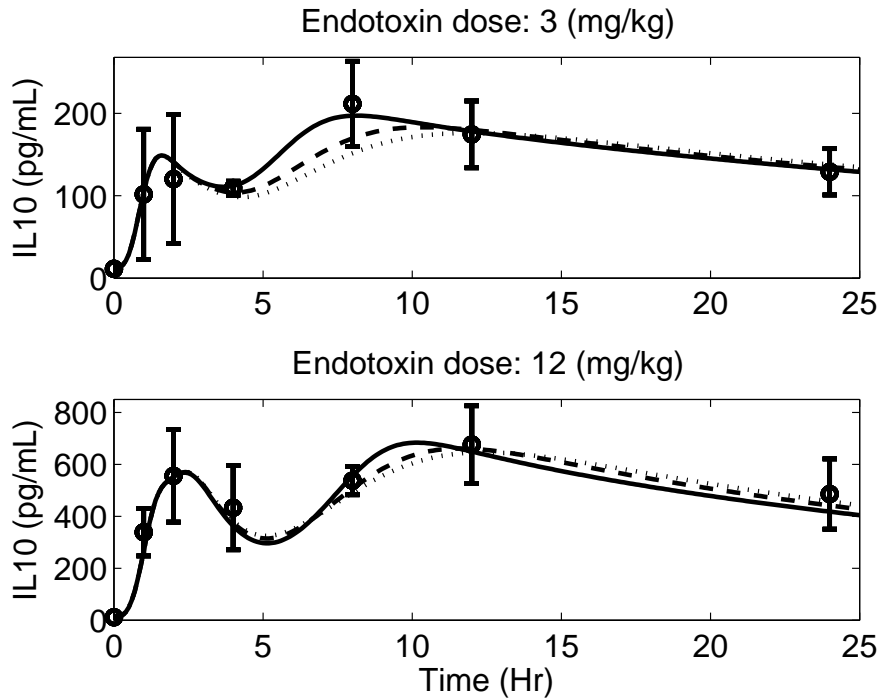


FIGURE 7. Model simulation comparison of damage-mediated IL-10 between the proposed model with a 6th-order Hill function in Eq. (20) (solid line), AV-7 with a 4th-order Hill function in Eq. (20) (dashed line), and AV-8 with a 2nd-order Hill function in Eq. (20) (dotted line) against experimental data (circle) (mean \pm SD) in response to endotoxin challenge of 3 mg/kg (top) and 12 mg/kg (bottom).

To accurately capture the $IL10(t)$ dynamics (20) at longer times for various endotoxin challenge levels, it was necessary to reduce the rate of elimination of $IL10(t)$ with increasing endotoxin dose level. This was achieved by introducing the down-regulating function, fDN_{IL10d} (Eq. (24)). The down-regulation in the model is physiologically motivated by studies showing that elevated levels of $IL10(t)$ reduce its own rate of elimination from the blood stream [22]. An alternate version

TABLE 2. Calculated AIC values of the proposed model and its alternate versions.

Model (Eq.)	Endotoxin Dose	
	3 mg/kg	12 mg/kg
IL-6 (10)	102.7	115.1
AV-1 (30)	120.9	123.3
AV-2 (31)	110.1	120.3
TNF (15)	96.0	102.0
AV-3 (32)	111.5	104.4
AV-4 (33)	108.6	102.7
IL-10 (20)	65.2	75.8
AV-5 (34)	88.2	90.4
AV-6 (35)	80.7	95.2
Effect of D on		
IL-10 (8)	65.2	75.8
AV-7	75.6	76.2
AV-8	81.9	77.5

of Eq. (20) without the fDN_{IL10d} function can be written as (AV-6):

$$\begin{aligned}
\frac{dIL10(t)}{dt} = & k_{IL10} \cdot \left(\frac{N(t)^3}{x_{IL10}^3 + N(t)^3} \right) \cdot [1 + k_{IL10IL6} \cdot fUP_{IL10IL6}(t) \\
& + k_{IL10TNF} \cdot fUP_{IL10TNF}(t)] - d_{IL10} \cdot IL10(t) \\
& + Y_{IL10}(t) + s_{IL10}
\end{aligned} \tag{35}$$

Due to the absence of the fDN_{IL10d} term, AV-6 has one less parameter (x_{IL10d}). Figure 5 shows the model prediction of $IL10(t)$ from AV-6 (dotted lines). Looking at the AIC values in Table 2, once again it is clear that the proposed model (20) is superior to both alternate versions.

3.4. Parameter Sensitivity Analysis. A parametric relative sensitivity matrix ($RS_{i,j}$) was generated using the finite difference method as described in Section 2.5. The matrix was comprised of 8 rows ($i \in [1,8]$), representing the states, and 46 columns ($j \in [1,46]$), representing all the parameters of the model. A graphical representation of the $RS_{i,j}$ values is provided in Figure 8. The x-axis lists parameters by number; this mapping is provided in Table 1. Each of the subplots in Figure 8 represent the parametric relative sensitivity values corresponding to a particular state (as shown in figure sub-titles). A higher $RS_{i,j}$ value indicates the state is more sensitive to the specified parameter.

In order to investigate the interactions between the various states of the proposed model, the parameters were grouped according to their association with each state, as indicated in Table 3. In Table 4, the contributions of each of these parameter groups, in terms of percentage relative sensitivity (%RS), to a particular state are listed. The %RS of a parameter group for each state is calculated by taking the sum of the relative sensitivity of each parameters in that particular group divided by the sum of relative sensitivity of the entire parameter set ($M = 46$) for that specific state.

It is evident from the %RS values of Table 4 that each state is sensitive to changes in its own parameters and the parameters associated with states $P(t)$ (as

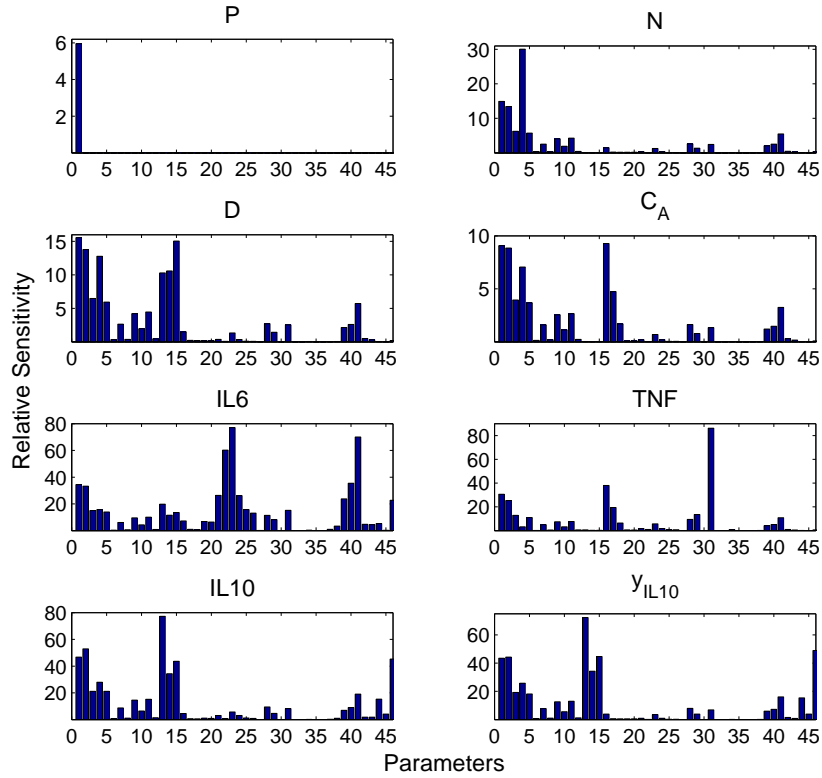


FIGURE 8. Parametric relative sensitivity analysis of the inflammation model for all the eight states.

TABLE 3. Parameters grouped according to their state association.

Parameter groups	Parameters
θ_P	d_p
θ_N	$k_N, x_N, d_N, k_{NP}, k_{ND}, x_{NTNF}, x_{NIL6}, x_{NCA}, k_{NTNF}, k_{NIL6}$
θ_D	k_D, d_D, x_D
θ_{C_A}	k_{CA}, d_{CA}, s_{CA}
θ_{IL6}	$k_{IL6TNF}, x_{IL6TNF}, k_{IL6}, d_{IL6}, x_{IL6}, x_{IL6IL10}, k_{IL6IL6}, x_{IL6IL6}, x_{IL6CA}$
θ_{TNF}	$k_{TNF}, d_{TNF}, x_{TNFIL10}, x_{TNFCA}, k_{TNFTNF}, x_{TNFTNF}, x_{TNFIL6}$
θ_{IL10}	$k_{IL10TNF}, x_{IL10TNF}, k_{IL10IL6}, x_{IL10IL6}, k_{IL10}, d_{IL10}, x_{IL10}, s_{IL10}, x_{IL10d}$
$\theta_{Y_{IL10}}$	$k_{IL102}, d_{IL102}, x_{IL102}$

endotoxin is the initiator) and $N(t)$ (as activated phagocytic cells are the primary driving force of the inflammatory action). In addition, the individual states are variably sensitive to other states when measured directly. The dynamics of the activated phagocytic cells, $N(t)$, are more sensitive to parameter changes associated

TABLE 4. Percentage relative sensitivity (%RS) of grouped parameters for each state.

States	% RS							
	θ_P	θ_N	θ_D	θ_{C_A}	θ_{IL6}	θ_{TNF}	θ_{IL10}	$\theta_{Y_{IL10}}$
$P(t)$	100	0	0	0	0	0	0	0
$N(t)$	14	65.1	0.2	1.8	2.3	6.0	10.2	0.4
$D(t)$	12.2	41.9	28.1	1.5	2.0	5.4	9.4	0.2
$C_A(t)$	13.2	46.7	0.1	23.0	2.0	5.4	9.4	0.2
$IL - 6(t)$	5.4	17.2	7.0	1.4	36.3	5.5	22.9	4.3
$TNF(t)$	9.6	24.2	0.4	20.0	4.1	34.6	6.9	0.2
$IL - 10(t)$	8.9	32.8	29.7	1.1	3.2	4.3	7.6	12.4
$Y_{IL10}(t)$	9.1	31.4	31.8	1.1	1.5	4	6.7	14.4

with $IL10(t)$ (θ_{IL10}), than to those of $IL6(t)$ (θ_{IL6}) and TNF (θ_{TNF}). State $IL6(t)$ also demonstrates higher sensitivity to parameters associated with $IL10(t)$ (θ_{IL10}) than TNF . For the $TNF(t)$ state, sensitivities to parameters associated with $C_A(t)$ (θ_{C_A}) are dramatically higher than $IL6(t)$ (θ_{IL6}) and $IL10(t)$ (θ_{IL10}). The $IL10(t)$ state and the unobserved filter, $Y_{IL10}(t)$ are primarily sensitive to parameters associated with $D(t)$ (θ_D) and the parameters of the unobserved state, $Y_{IL10}(t)$. Other cytokine state parameters show lower sensitivity to $IL - 10(t)$ directly, although they likely drive systemic anti-inflammatory response through secondary effects via $N(t)$ and $D(t)$.

4. Discussion. This work extends a previously developed 3-D model of the acute inflammatory response to pathogen or endotoxin to an 8-D differential equation model of the acute inflammatory response system, primarily by representing the dynamics of a variety of specific cytokines previously treated as more abstract factors. Model parameter values were calibrated to achieve a close fit, in the least-squares sense, to longitudinal rat data for 3 of the 8 state variables, which were measured following endotoxin dose challenges at 3 mg/kg and 12 mg/kg . Moreover, with these fixed parameter values, the model predicted the response to an intermediate endotoxin challenge of 6 mg/kg . The model also described the time course of the unobserved activation of phagocytic cells by endotoxin, as well as unaccessible variables, like tissue damage (D) caused by the activated phagocytic cells and the slow-acting anti-inflammatory mediator (C_A). The data and the resulting model response display significant nonlinearity across the three challenge levels. Hence, the accurate prediction of the intermediate dose without the need for additional parameter or parameter value changes supports the validity of the model structure, as well as its interpolative, and possibly extrapolative, utility.

Improving biological fidelity and reproducing data accurately were of prime importance in this work; care was taken that the added complexity reflected known inflammatory physiology. This came at a cost of a considerable increase in the number of equations and parameters. This exercise is representative of the ongoing challenge of balancing biological fidelity, often yielding large equation dimension and highly parameterized models, with accuracy of, and confidence in, model parameters based on fits to experimental data. Unlike chemical or physical interactions, which are generally well characterized, biological interactions are often poorly quantified and causality is often not established with certainty. Hence, the problem of

synthesizing and identifying the simplest system that can be expected to provide reasonable quantitative predictions is difficult and pervasive. System simplicity can be debated on (non)linear, dimensional, and parametric grounds, even without the added complexity of dynamics, where time is the independent variable. In the present case, we opted to minimize the number of state variables and to avoid explicit time delays; the price was increased nonlinearity in the model. It could be argued that one should always strive to minimize nonlinearity. Clearly, the inclusion of additional intermediates (first-order filter equations) or explicit delays would have significantly reduced the need for Hill equation-type nonlinearities. It could also be argued that our use of sigmoidal activation functions is not rooted on any demonstrable co-operativity phenomena. In their favor, these functions avoid the use of pure delays, which present additional challenges to simulators and optimization algorithms, without significantly increasing the number of parameters that must be identified.

Beyond model structure is the evaluation of model performance – how well does the model fit or predict the data? The present model generates substantially better fits than those obtained with our previous models [6, 3]. A critique of our fitting efforts could be our lack of a 12-hour time point, which would allow for a better characterization of the later phase of the inflammatory dynamics. Unfortunately it was impractical to maintain personnel overnight for that purpose. In synthesizing the model, we found that appropriate interdisciplinary input, from expert inflammation biologists and experimentalists, was of great value in determining appropriate experimental time points and in defining heuristically appropriate behavior of the model. The term “heuristically appropriate” refers to the process of defining biologically motivated or consistent accessory constraints to assist the parameter estimation process. For example, since all animals survived the insult, we imposed the constraint that damage asymptotically returned to zero. Similarly, parameter ranges explored by the fitting algorithm were restricted based on inferences from the literature or expert opinion.

Parameter fitting was performed using a gradient-based optimization routine. Given the nonlinear nature and ill-posedness of parameter estimation from data for dynamic models, it can be expected that other parameter sets could have yielded fits of similar quality. Lower-dimensional models will typically have smoother objective functions due to the monotonic nonlinearities used in the model and the smaller number of parameters requiring identification. Hence, reducing the number of non-identifiable parameters should result in a smaller number of different parameter sets yielding high-quality fits. Much like statistical models, parsimony may improve the chances of broader validity, yet it usually results in a decreased ability to fit data well. However, contrary to statistical modeling, parsimony cannot overrule biological plausibility, as broader validity of biological models is rooted in their ability to represent mechanisms active in the biological system. Accordingly, there is no preferred technique to reduce biologically-motivated dynamical models beyond taking advantage of time scale differences and algebraic dependencies.

A logical first step in reducing parameter dimension in a nonlinear model is parametric sensitivity analysis, with sensitivities calculated at all available time points. Insensitivity implies that either the parameter is varied outside of the biologically relevant range, or the biology represented by the insensitive parameter does not impact the outcome of interest in a significant way. Because of the first possibility, insensitivity should not immediately dictate model reduction. High sensitivity, on

the other hand, may help guide model reduction [29], specifically when sensitivities between two parameters are correlated. Accordingly, such prediction is most appropriate if sensitivity is observed to be consistent across parameter sets of an ensemble of fits to a given dataset [31]. Model reduction techniques arguably stand on firmer ground if such a consistency is observed. The ultimate goal of our model development and fitting efforts is to create an ensemble of models that reflect, given the variability of the observed data, the range of parameter sets that could have generated this data (see also [31]).

In contrast to the biologically-motivated, but heuristic, approach to model structure analysis and parameter identification discussed above, a mathematically rigorous analysis of the experiment would have the ability to establish shortcomings in the model-data combination, leading to changes in either the model or experiment to better couple the model and data. A formal test of a model structure and data set for well-posedness of the parameter estimation problem is to evaluate the *a priori* identifiability of the model given the data [33, 35, 34]. The theory states that a model is *a priori* identifiable if, under the ideal conditions of noise free measurements and error free model structure, the unknown parameters of the proposed model can be uniquely recovered from the measured data collected during the experiment [33]. A variety of methods have been developed for (non)linear *a priori* global identifiability, including power series [36], similarity transform [35], and differential algebra [34, 37]. The recent work of [37] employs Gröbner basis techniques to evaluate identifiability for nonlinear polynomial (or rational) systems; given the class of saturating nonlinearities used in the present work, a detailed analysis of the proposed model via functional approximation or another transformation is beyond the scope of the present work.

In summary, we propose that the development of top-down models of biological processes that target quantitative validation and prediction should: (i) primarily reflect known biological interactions among model components; (ii) be developed by interdisciplinary teams where data collection is planned with modeling as a primary consideration; and (iii) apply relevant literature and appropriate heuristics, based on experimental observations, to guide model development. Thereafter, sensitivity and identifiability analysis-guided model reduction (both dimensional and parametric) can be employed to reduce model complexity. Finally, ensemble creation and validation on separate datasets are necessary steps to the formulation of biologically relevant, quantitatively accurate dynamical models of complex processes.

Acknowledgments. Funding for this work was provided by the NIH NHLBI #1R01HL080926.

REFERENCES

- [1] C. Nathan, *Points of control in inflammation*, Nature, **420** (2002), 846–852.
- [2] I. Mackay and F. S. Rosen, *Advances in immunology* N. Engl. J. Med., **343** (2000), 338–344.
- [3] J. Day, J. Rubin, Y. Vodovotz, C. C. Chow, A. Reynolds, and G. Clermont, *A reduced mathematical model of the acute inflammatory response II. Capturing scenarios of repeated endotoxin administration*, J. Theor. Biol., **242** (2006), 237–256.
- [4] R. J. Goris, T. P. te Boekhorst, J. K. Nuytinck, J. S. Gimbrere, *Multiple-organ failure. Generalized autodestructive inflammation?*, Arch. Surg., **120** (1985), 1109–1115.
- [5] P. Y. Bochud and T. Calandra, *Pathogenesis of sepsis: new concepts and implications for future treatment*, B. M. J., **326** (2003), 262–266.
- [6] R. Kumar, G. Clermont, Y. Vodovotz, and C. C. Chow, *The dynamics of acute inflammation*, J. Theor. Biol., **230** (2004), 145–155.
- [7] C. C. Chow, G. Clermont, R. Kumar, C. Lagoa, Z. Tawadrous, D. Gallo, B. Betten, J. Bartels, G. Constantine, M. P. Fink, T. R. Billiar, and Y. Vodovotz, *The Acute inflammatory response in diverse shock states*, Shock, **24** (2005), 74–84.
- [8] J. M. Prince, R. M. Levy, J. Bartels, A. Baratt, J. M. Kane III, C. Lagoa, J. Rubin, J. Day, J. Wei, M. P. Fink, S. M. Goyert, G. Clermont, T. R. Billiar, and Y. Vodovotz, *In silico and in vivo approach to elucidate the inflammatory complexity of CD14-deficient mice*, Mol. Med., **12** (2005), 88–96.
- [9] C. E. Lagoa, J. Bartels, A. Baratt, G. Tseng, G. Clermont, M. P. Fink, T. R. Billiar, and Y. Vodovotz, *The role of initial trauma in the host's response to injury and hemorrhage: Insights from a correlation of mathematical simulations and hepatic transcriptomic analysis*, Shock **26** (2006), 592–600.
- [10] A. Reynolds, J. Rubin, G. Clermont, J. Day, Y. Vodovotz, and G. B. Ermentrout, *A reduced mathematical model of the acute inflammatory response. I. Derivation of model and analysis of anti-inflammation*, J. Theor. Biol., **242** (2006), 220–236.
- [11] F. A. Bozza, J. I. Salluh, A. M. Japiassu, M. Soares, E. F. Assis, R. N. Gomes, M. T. Bozza, H. C. Castro-Faria-Neto, and P. T. Bozza, *Cytokines profiles as markers of disease severity in sepsis: a multiplex analysis*, Critical Care, **11(2)** (2007), R49.
- [12] B. D. Freeman and C. Natanson, *Anti-inflammatory therapies in sepsis and septic shock*, Expert Opin. Investig. Drugs, **9** (2000), 1651–1663.
- [13] J. S. Hadley, J. E. Wang, S. J. Foster, C. Thiemermann, and C. J. Hinds, *Peptidoglycan of staphylococcus aureus upregulates monocyte expression of CD14, toll-like receptor 2 (TLR2), and TLR4 in human blood: possible implications for priming of lipopolysaccharide signaling*, Infection and Immunity, **73(11)** (2005), 7613–7619.
- [14] G. Bellingan, *Inflammatory cell activation in sepsis*, Br. Med. Bull., **55** (1999), 12–29.
- [15] M. Pretolani, *Interleukin-10: an anti-inflammatory cytokine with therapeutic potential*, Clin. Exp. Allergy, **29** (1999), 1164–1171.
- [16] M. R. Pinsky, *Sepsis: a pro- and anti-inflammatory disequilibrium syndrome*, Contrib. Nephrol., **132** (2001), 354–366.
- [17] D. Rittirsch, L. Marco Hoesel, and P. A. Ward, *The disconnect between animal models of sepsis and human sepsis*, J. Leukoc. Biol., **81** (2007), 137–143.
- [18] P. Matzinger, *The danger model: a renewed sense of self*, Science, **296** (2002), 301–305.
- [19] P. V. Giannoudis, R. M. Smith, S. L. Perry, A. J. Windsor, R. A. Dickson, and M. C. Bellamy, *Immediate IL-10 expression following major orthopaedic trauma: relationship to anti-inflammatory response and subsequent development of sepsis*, Intensive Care Med., **26(8)** (2000), 1076–1081.
- [20] K. Kamm, W. Vanderkolk, C. Lawrence, M. Jonker, and A. T. Davis, *The effect of traumatic brain injury upon the concentration and expression of interleukin-1beta and interleukin-10 in the rat*, J. Trauma, **60(1)** (2006), 152–157.
- [21] Z. Xing Z, J. Gaudie, G. Cox, H. Baumann, M. Jordana, X. F. Lei, M. K. Achong, *IL-6 is an antiinflammatory cytokine required for controlling local or systemic acute inflammatory responses*, J. Clin. Invest., **101(2)** (1998), 311–320.
- [22] I. Y. Rosenblum, R. C. Johnson, and T. J. Schmahai, *Preclinical safety evaluation of recombinant human interleukin-10*, Regulatory Toxicology and Pharmacology, **35(1)** (2002), 56–71.

- [23] M. J. P. Lenczowski, A. M. Van Dam, S. Poole, J. W. Larrick, and F. J. Tilders, *Role of circulating endotoxin and interleukin-6 in the ACTH and corticosterone response to intraperitoneal LPS* Tilders, *Am. J. Physiol. Regul. Integr. Comp. Physiol.*, **273** (1997), 1870–1877.
- [24] M. H. Iversen and R. G. Hahn, *Acute effects of vitamin A on the kinetics of endotoxin in conscious rabbits*, *Intensive Care Med.*, **25** (1999), 1160–1164.
- [25] A. E. Warner, M. M. DeCamp Jr., R. M. Molina, and J. D. Brain, *Pulmonary removal of circulating endotoxin results in acute lung injury in sleep*, *Lab. Invest.*, **59** (1988), 219–230.
- [26] E. Carson and C. Cobelli, “Modelling methodology for physiology and medicine”, Academic Press, San Diego, CA, 2001.
- [27] H. Akaike, *A bayesian extension of the minimum AIC procedure of autoregressive model fitting*, *Biometrika*, **66** (1979), 237–242.
- [28] H. Yue, M. Brown, J. Knowles, H. Wang, D. S. Broomhead, and D. B. Kell, *Insights into the behaviour of systems biology models from dynamic sensitivity and identifiability analysis: a case study of an NF- κ B signalling pathway*, *Mol. Biosyst.*, **2** (2006), 640–649.
- [29] D. E. Zak, G. E. Gonye, J. S. Schwaber, and F. J. Doyle III, *Importance of input perturbations and stochastic gene expression in the reverse engineering of genetic regulatory networks: insights from an identifiability analysis of an in silico network*, *Genome Res.*, **13** (2003), 2396–2405.
- [30] S. Daun, R. S. Parker, A. Roy, J. Rubin, and G. Clermont, *Parameter identifiability in a model of the acute inflammatory response*, *J. Crit. Care*, **22(4)** (2007), 345.
- [31] S. Daun, J. Rubin, Y. Vodovotz, A. Roy, R. Parker, and G. Clermont, *An ensemble of models of the acute inflammatory response: results from parameter reduction*, *J. Theor. Biol.*, **253** 2008, 843–853.
- [32] B. Hancioglu, G. Clermont, and D. Swigon, *Ensemble models for human immune response to influenza A virus infection*, *J. Crit. Care*, **22(4)** (2007), 339.
- [33] S. Audoly, L. D. Angio, M. P. Saccomani, and C. Cobelli, *Global identifiability of linear compartmental models*, *IEEE Trans. Biomed. Eng.*, **45** (1998), 36–47.
- [34] L Ljung and S. T. Glad, *On global identifiability for arbitrary model parameterizations*, *Automatica*, **30(2)** (1994), 265–276.
- [35] M. J. Chappel and K. R. Godfrey, *Structural identifiability of the parameters of a nonlinear batch reactor model*, *Math. Biosci.*, **108** (1992), 245–251.
- [36] H. Pohjanpalo, *Systems identifiability based on the power series expansion of the solution*, *Math. Biosci.*, **41** (1978), 21–33.
- [37] S. Audoly and G. Bellu and L. D. Angio and M. P. Saccomani and C. Cobelli, *Global identifiability of nonlinear models of biological systems*, *IEEE Trans. Biomed. Eng.*, **48(1)** (2001), 55–65.

E-mail address: rparker@pitt.edu